JCTC Journal of Chemical Theory and Computation

A Base-Sugar−Phosphate Three-Layer ONIOM Model for Cation Binding: Relative Binding Affinities of Alkali Metal Ions for Phosphate Anion in DNA

Neethu Sundaresan[†] and Cherumuttathu H. Suresh*[,‡]

Chemical Sciences and Technology Division and Computational Modeling and Simulation Section, Regional Research Laboratory (Council of Scientific and Industrial Research), Trivandrum 695019, India

Received July 28, 2006

Abstract: A three-layer ONIOM approach was used to study the interactions of hydrated alkali metal ions such as Li^+, Na^+, and K^+ with a DNA fragment containing two phosphate groups, three sugar units, and a G••C base pair modeled in the anion and dianion states. Among the three metal-binding combinations studied herein (outer-sphere, inner-sphere monodentate, and inner-sphere bidentate), the outer-sphere binding mode showed the highest binding energy (BE) for hydrated Li^+ ions (103.1 kcal/mol) while the hydrated Na^+ and K^+ ions preferred the inner-sphere monodentate binding modes to the phosphate group of the anionic DNA fragment (BE = 87.9 and 98.2 kcal/mol for Na^+ and K^+, respectively). These data on the binding mechanisms of Li^+, Na^+, and K^+ ions and the higher binding affinity of Li^+ ions compared to Na^+ and K^+ ions in the anion model system of DNA are in good agreement with the previous experimental findings. On the other hand, in the dianion state, Li^+ preferred inner-sphere monodentate, whereas Na^+ and K^+ ions preferred the outer-sphere structures. The neutral anion model ion revealed a more realistic picture of DNA−alkali metal ion interactions compared to the non-neutral dianion model systems.

I. Introduction

DNA, the highly anionic polyelectrolyte in a living cell, is stabilized by an array of cationic species, including metal ions. Metal cations are known to play a crucial role in both stabilizing and destabilizing the DNA double helix.[1−4] They can coordinate DNA at several sites, of which the major sites are the phosphate groups, the sugar moiety, the base keto oxygens (O2 of thymine and O6 of guanine on the interior of the double helix), and the ring nitrogens (N7 of adenine and guanine on the exterior and N3 of adenine and guanine) (see Figure 1), the different coordinations depending on the concentration and type of metal ions. The affinity of a cation for a specific site on a polynucleotide is a general function of its charge, hydration-free energy, coordination geometry, and coordinate bond-forming capacity.[5,6] Both alkali and alkaline earth metal ions are known to stabilize the DNA predominantly by neutralizing the negatively charged sugar−phosphate backbone.[7−9] Coordination of phosphate moieties by cations is essential for catalytic enzymatic reactions, the processes involving the transfer of genetic information and the synthesis of oligonucleotides and so forth.[10,11]

The DNA−metal ion interactions are governed by several parameters such as the nature of the metal, its size, and its charge, which influence the conformation of DNA by direct or indirect interaction through the water molecules with the basic sites of the nucleotides.[12] As monovalent cations are generally less strongly solvated than divalent cations, they tend to interact with DNA purely electrostatically without making hydrogen bonds from metal-coordinated water molecules.[13]

Molecular dynamic (MD) simulations, solution NMR, and crystallographic results agree that the monovalent cations

* Corresponding author e-mail: sureshch@gmail.com
[†] Chemical Sciences and Technology Division.
[‡] Computational Modeling and Simulation Section.

10.1021/ct600245w CCC: $37.00
Published on Web 04/19/2007

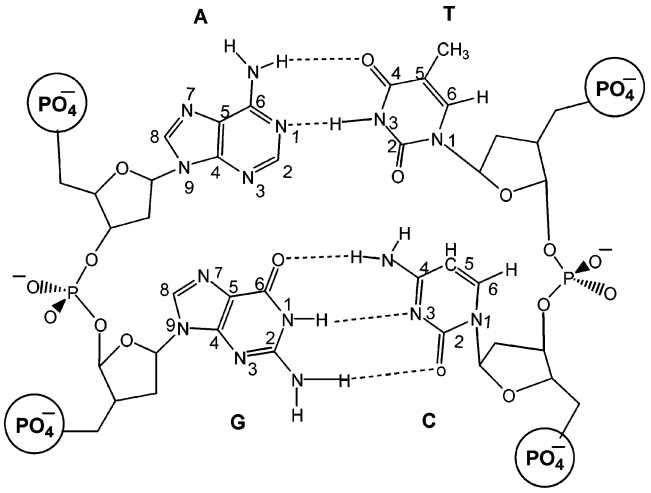

Figure 1. Schematic diagram of A••T and G••C base pairs linked by phosphate groups.

Na^+, K^+, Rb^+, and Cs^+ prefer direct binding (inner-sphere) at the ApT step in the A-track in the minor groove of DNA.[14,15] Li^+ is reported to interact with the minor groove via a water bridge.[16]

A recent study carried out by Wilson and co-workers on MD simulations of 10 ns and longer on DDD (Dickerson−Drew dodecamer with sequence CGCGAATTCGCG),[17] and by Feig and Pettitt on the DNA duplex (A5G5)•(C5T5), with Na^+ as the counterion observed a correlation between the entrance of Na^+ into the minor groove and groove narrowing.[18] Among the alkali metal ions, Na^+ and K^+ are widely distributed in most of the biological systems and are involved in a variety of cellular functions.[19]

Most of the previous theoretical studies devoted to metal−DNA binding by Sponer et al.,[20−25] Petrov et al.,[26−28] and other groups[29−36] were carried out on small model systems such as base pairs, nucleotides, dimethyl phosphate anions, solvated metal ions, and so forth, could shed new insights into the mechanisms of metal binding to nucleic acids. In native DNA, the electronegative oxygen atoms of the phosphate group are projected toward the exterior of the double helix, and the small models are largely ineffective in replicating such geometrical constraints.

So, it was thought worthwhile that a study with a model system where negative oxygen atoms of the phosphate group project toward the exterior would be more comparable to the native DNA structure. In the present study, the selected model is a guanine−cytosine base-pair region (G••C region), which also contains the related two sugar units (one connected to the guanine fragment and the other connected to cytosine fragment) and the associated two phosphate groups (one free anionic phosphate group at the cytosine end, which is the anion model). Because of the structural restrictions imposed by the sugar units, we hope that in the present model the phosphate geometry will be maintained as in native DNA. DNA being an anionic polyelectrolyte, one would expect excess negative charge on the DNA segments. Therefore, to compare the effect of excess charge on DNA fragments on the interactions of alkali metal ions with DNA, besides the anion model, we have considered a dianionic model possessing two negative phosphate ends. In the present work, we have adopted a three-layer ONIOM method [a hybrid of quantum mechanical and molecular mechanics methods (QM−MM)] to study the interaction of hydrated alkali metal ions with the anionic and dianionic DNA fragments. As negatively charged phosphate groups are the major contributors to the polyanionic nature of the DNA macromolecule, the present study will mainly be focused on the interaction of biologically important metal ions such as Li^+, Na^+, and K^+ ions with the phosphate groups of DNA.

II. Computational Details and Models

A. Three-Layer ONIOM Model. In this work, we will be utilizing a three-layer ONIOM method, developed by Morokuma and co-workers,[37−39] to study the metal ion interactions with the DNA segment. ONIOM is a general hybrid method, which can combine molecular orbital as well as molecular mechanics methods, and it is reported to be an efficient tool for accurately calculating chemical interactions in large systems.[40,41]

In the present study, a typical system used for ONIOM calculation is given in Figure 2. We name this model HPSG••CSP^-••M^+_{hyd}, where HP stands for the protonated phosphate group at the guanine end, SG stands for the sugar and the connected guanine, the doted line indicates the hydrogen-bond interaction between the guanine and cytosine, CSP^- stands for the cytosine and the connected sugar units and the phosphate anion, M^+_{hyd} is the hydrated metal ion, and the dotted line between CSP^- and M^+_{hyd} represents the interaction between the two units. In the case of alkali metal ions, typically, four water molecules are found in their first solvation shell, and accordingly we use the $M^+(H_2O)_4$ model for the hydrated metal ion (for selected cases, higher coordination possibilities of the metal ions are also modeled). It may be noted that, in the HPSG••CSP^-••M^+_{hyd} model, the net charge is zero. Therefore, in order to study the effect of excess charge on the M^+_{hyd}−DNA interactions, we have also studied a dianion model which is designated as $(H_2O)_2$••$^-$PSG••CSP^-. Here also, an ONIOM model similar to the one in Figure 2 is used, wherein the P^- at the cytosine end is in the high level and the P^- at the guanine end is in the medium level. In order to have a realistic picture, the guanine end is microsolvated with a water dimer, which is also in the medium layer. According to the ONIOM terminology, the model HPSG••CSP^-••M^+_{hyd} is divided into three layers, namely, (i) a high layer, (ii) a medium layer, and (iii) a low layer, which are illustrated in Figure 2. The high layer contains the critical part of the reacting system, namely, the phosphate group and interacting hydrated metal ion, which is treated at the B3LYP/6-31G(d) level of density functional theory (DFT).[42−44] The G••C base pair, the sugar units, and the phosphate group at the guanine end were treated at the medium level of theory by using the semiempirical PM3 method.[45] The use of the PM3 method in the medium layer will incorporate some electronic effects into the system, and it will also help the delocalization of the charge centered on the phosphate moieties. The sugar units in the low layer are treated with a universal force field.[46] Since there are no electrons in the MM layer, the phosphate

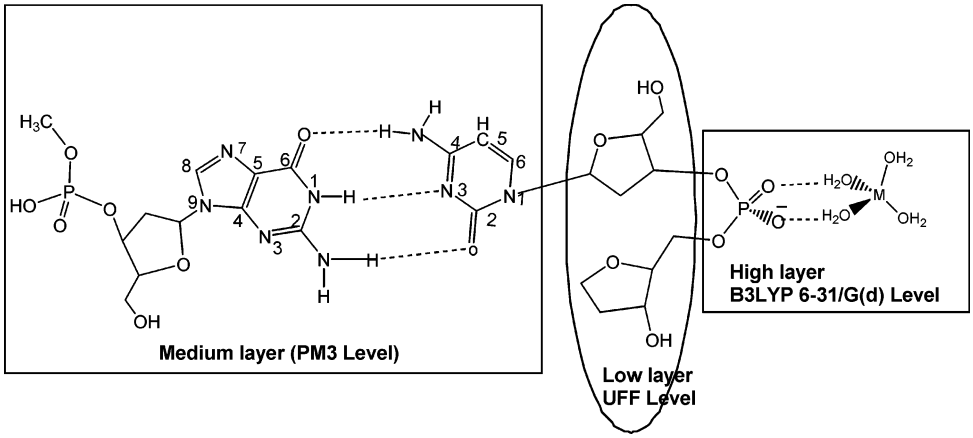

Figure 2. Scheme of the real and model systems used in the ONIOM calculations for DNA−hydrated-metal interaction.

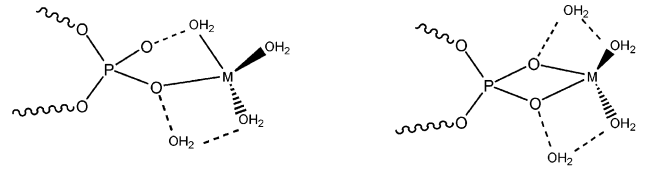

Figure 3. Scheme of the different binding modes selected to study hydrated alkali metal ions and phosphate anion interactions.

group will not interact electronically with this layer, and therefore great twisting of the phosphate groups leading to phosphate and G••C interaction may be prevented. Great twisting of the phosphate groups is less likely to occur in DNA molecules because of the rigid double-stranded structure. Therefore, we expect that the steric effect imposed by the sugar unit can be retained in the MM layer, and at the same time, the direct electronic interaction between the QM layer and the medium layer can be prevented, which in turn will help the phosphate moiety to project toward the exterior of the DNA fragment. Therefore, it is felt that the three-layer ONIOM model will serve as a good model for the study of phosphate and hydrated-metal ion interactions in DNA systems. For interaction energy calculations, structures of hydrated metal ions are fully optimized at the B3LYP/6-31G(d) level of theory (see the Supporting Information, SI, for the structures).

The binding mode given in Figure 2 is the outer-sphere combination of the hydrated metal and the phosphate group. Inner-sphere monodentate and inner-sphere bidentate combinations (Figure 3) are also commonly observed in metal-binding interactions with electron-rich centers. It may be noted that, in the models given in Figure 3, one or two water molecules will have to move out from the tetra-hydration shell of the metal (one for mono- and two for bidentate) to make room for the direct metal−phosphate oxygen bonds. This assumption is reasonable because alkali metal ions prefer three to four metal−oxygen direct bond connections. For instance, in a theoretical study of alkali metal ion−water interaction conducted with models of $M^+(H_2O)n$, Glendeing and Feller[47] have found that, for larger clusters ($n = 4-6$), one or two water molecules often occupy the secondary solvation shell.[9,14,48] The possibilities of higher coordination geometries for the metal ions will also be considered to a limited extent.

B. Interaction Energy Calculations. In the present calculations, the following geometry types are optimized with the three-layer ONIOM method, namely, (i) the bare anion HPSG••CSP^-, (ii) the bare dianion $(H_2O)_2$••$^-$PSG••CSP^-, (iii) the metal−anion HPSG••CSP^-••$M^+(H_2O)_4$, and (iv) the metal−dianion $(H_2O)_2$••$^-$PSG••CSP^-••$M^+(H_2O)_4$ systems. In type i and type ii geometries, the main interaction is between the bases G and C, while in types iii and iv structures, both the base pair interaction and the hydrated metal ion and phosphate anion interaction occur. Therefore, we can estimate the following interaction energies.

For G••C base pair interaction energy in the free anion

$$\mathrm{E1} = E(HPSG) + E(CSP^-) - E(\mathrm{HPSG{\bullet\bullet}CSP^-}) + \mathrm{E1_{BSSE}} \quad (1)$$

For G••C base pair interaction energy in the bare dianion

$$\mathrm{E2} = E[(H_2O)_2{\bullet\bullet}^-PSG] + E(CSP^-) - E[(\mathrm{H_2O})_2{\bullet\bullet}^-\mathrm{PSG{\bullet\bullet}CSP^-}] + \mathrm{E2_{BSSE}} \quad (2)$$

For G••C base pair interaction energy in the metal bound anion systems

$$\mathrm{E3} = E(HPSG) + E(CSP^-{\bullet\bullet}\mathrm{M^+_{hyd}}) - E(\mathrm{HPSG{\bullet\bullet}CSP^-{\bullet\bullet}M^+_{hyd}}) + \mathrm{E3_{BSSE}} \quad (3)$$

For G••C base pair interaction energy in the metal bound dianion systems

$$\mathrm{E4} = E[(H_2O)_2{\bullet\bullet}^-PSG] + E(CSP^-{\bullet\bullet}\mathrm{M^+_{hyd}}) - E[(\mathrm{H_2O})_2{\bullet\bullet}^-\mathrm{PSG{\bullet\bullet}CSP^-{\bullet\bullet}M^+_{hyd}})] + \mathrm{E4_{BSSE}} \quad (4)$$

For metal ion−phosphate interaction energy in the anion systems

$$\mathrm{E5} = E(\mathrm{HPSG{\bullet\bullet}CSP^-}) + \mathrm{E(M^+_{hyd})} - E(\mathrm{HPSG{\bullet\bullet}CSP^-{\bullet\bullet}M^+_{hyd}}) + \mathrm{E5_{BSSE}} \quad (5)$$

For hydrated metal ion−phosphate interaction energy in the dianion systems

$$E6 = E[(H_2O)_2 \bullet\bullet^- PSG \bullet\bullet CSP^-] + E(M^+_{hyd}) - E[(H_2O)_2 \bullet\bullet^- PSG \bullet\bullet CSP^- \bullet\bullet M^+_{hyd}] + E6_{BSSE} \quad (6)$$

E is the total energy of the systems given in parenthesis. In order to get a reasonable estimate of the *E* values, the single-point energies of the ONIOM-optimized structures of all the anionic ($HPSG \bullet\bullet CSP^- \bullet\bullet M^+_{hyd}$) and dianionic [$(H_2O)_2 \bullet\bullet^- PSG \bullet\bullet CSP^- \bullet\bullet M^+_{hyd}$] systems are calculated at the B3LYP/6-31G(d) level. Further, *E* values at the B3LYP/6-31G (d) level are calculated for the fragment structures HPSG, $(H_2O)_2 \bullet\bullet^- PSG$, and CSP^- taken from their respective full systems. Names in regular font are of the fully optimized ONIOM level structures, and those in italics are of the fragment structures taken from the fully optimized systems. The $E1_{BSSE}$ to $E6_{BSSE}$ values are the BSSE corrections to be obtained by employing the counterpoise correction method of Boys and Bernardi.[49] The BSSE-corrected interaction energy is used for comparing the stability of different structures.

III. Results and Discussion

A. Bare Anion and Dianion Models of a DNA Fragment. The ONIOM-level-optimized geometries of the bare anion and dianion models of the DNA fragment are given in Figure 4a and b, respectively. As expected, in the optimized geometries, the P−O bonds that are not connected to the sugar units are projected outward with respect to the G••C base pair. The low level of MM theory proved useful, particularly to treat the steric effect of these sugar units, which are mainly responsible for this structural feature. The extra electrons in the systems are delocalized over the exposed P−O bonds, and as a result, they show more double-bond character than the P−O bonds connected to the sugar units. For instance, in the QM layer, the exposed P−O distance is in the range of 1.498−1.501 Å, while the P−O bond connected to the sugar unit is in the range of 1.700−1.712 Å. In DNA systems, the P−O bonds showing double-bond character are typically seen at a distance of 1.48−1.51 Å, and the present results are in good agreement with this. However, the distance obtained for the P−O bond connected to the sugar unit is larger than the typically observed value in the range of 1.59−1.64 Å in DNA systems[50,51] (later, we will see better values for the longer P−O bond distances in systems containing hydrated metal ions). Shortening of the P−O bond length is mainly due to strong solvation or a counterion effect in DNA systems.

Although understanding the nature of interactions between the DNA phosphate group and the alkali metal ion was the primary objective of the present work, the ONIOM models used in the current study could also provide information on the stability of the G••C base pair in the anion, dianion, and their metal-containing systems. This is possible because the PM3 method, being well-parametrized for organic molecules, applied at the G••C base pair region can yield reliable structural features. For instance, in both the anion and dianion models, the aromatic rings of the G••C base pair are nearly in the same plane, which agrees well with the planar G••C structures often found in DNA systems. Further, the hydrogen-bond length parameters obtained for the G••C base pair region show good agreement with the results obtained by Sponer et al. at the RI-MP2/TZVPP level (a planar structure with $O6_{(G)}-N4_{(C)} = 2.750$ Å, $N1_{(G)}-N3_{(C)} = 2.900$ Å, and $N2_{(G)}-O2_{(C)} = 2.891$ Å).[52] Moreover, for a free G••C base pair optimized at the PM3 level, the distances obtained for the $O6_{(G)}-N4_{(C)}$, $N1_{(G)}-N3_{(C)}$, and $N2_{(G)}-O2_{(C)}$, are 2.813, 2.800, and 2.850 Å, respectively, and the corresponding values obtained for the anion and dianion models are nearly the same. The distances observed for the ordered triplet ($O6_{(G)}-N4_{(C)}$, $N1_{(G)}-N3_{(C)}$, $N2_{(G)}-O2_{(C)}$) in the G••C base pair for free anion and dianion models are (2.820, 2.804, 2.828 Å) and (2.810, 2.814, 2.847 Å), respectively, suggesting that the hydrogen-bond interactions at the $N1_{(G)}-N3_{(C)}$ and $N2_{(G)}-O2_{(C)}$ regions in the dianion model are weaker than that found in the anion model, which can be attributed to the enhanced electrostatic repulsive interaction arising from anionic guanine and anionic cytosine ends. Further, a well-defined water dimer interaction is also present in the guanine end of the dianion model, which would provide a microsolvation environment to the phosphate moiety. It may be noted that, in the case of both anion and dianion models, the bond lengths $N_{(G)}-C_{(sugar)}$, $N_{(C)}-C_{(sugar)}$, and $C_{(sugar)}-O_{(phosphate)}$ observed at the boundary that separates the QM layer from the MM layer (DFT/MM and PM3/MM boundaries) are in good agreement with the corresponding distances in the DNA systems (Figure 4).

In the free anion and dianion models, the BSSE-corrected G••C base pair interaction energy values are calculated according to eqs 1 and 2, respectively, and a value of E1 = 29.6 kcal/mol for the anion and E2 = 7.3 kcal/mol for the dianion is obtained.[53] These values are already reported in a recent article, and the smaller base pair interaction energy in the dianion model is attributed to the repulsive electrostatic interaction between the negatively charged guanine and the negatively charged cytosine fragments.

B. Anion and Dianion Models for Hydrated Alkali Metal Ion Interactions. *Geometries of HPSG••CSP$^-$ ••M$^+$(H$_2$O)$_4$ Anion Models.* The binding of alkali metal ions such as Li^+, Na^+, and K^+ to the anionic phosphate group in the anion model with different binding mechanisms is optimized at the ONIOM level according to the scheme given in Figures 2 and 3. In these models, the primary solvation shell of the metal ion is modeled with four water molecules because, normally, tetrahydration is observed in alkali metal ions (see the SI for a discussion on the hydrated structures of metal ions).[47] In Figure 5a, the full optimized geometry for the outer-sphere coordination of $Li^+(H_2O)_4$ with the $HPSG \bullet\bullet CSP^-$ model is depicted. In order to have a closer look at the hydrated metal region interacting with the phosphate anion, the QM region of the ONIOM optimized geometry of the outer-sphere coordination of $Li^+(H_2O)_4$ is also presented in Figure 5b. Only the QM regions in the cases of inner-sphere monodentate and bidentate structures of Li^+ are presented in Figure 5c and d, respectively (see SI for the full geometry). In all three of the binding modes, Li−O bonds are more or less in a tetrahedral arrangement. In mono- and bidentate structures, Li−O bonds to the water molecule (1.950, 1.961, 1.985, 1.912, and 1.933 Å) are shorter than the Li−O bonds to the phosphate oxygen (2.010, 2.141, and 2.160 Å).

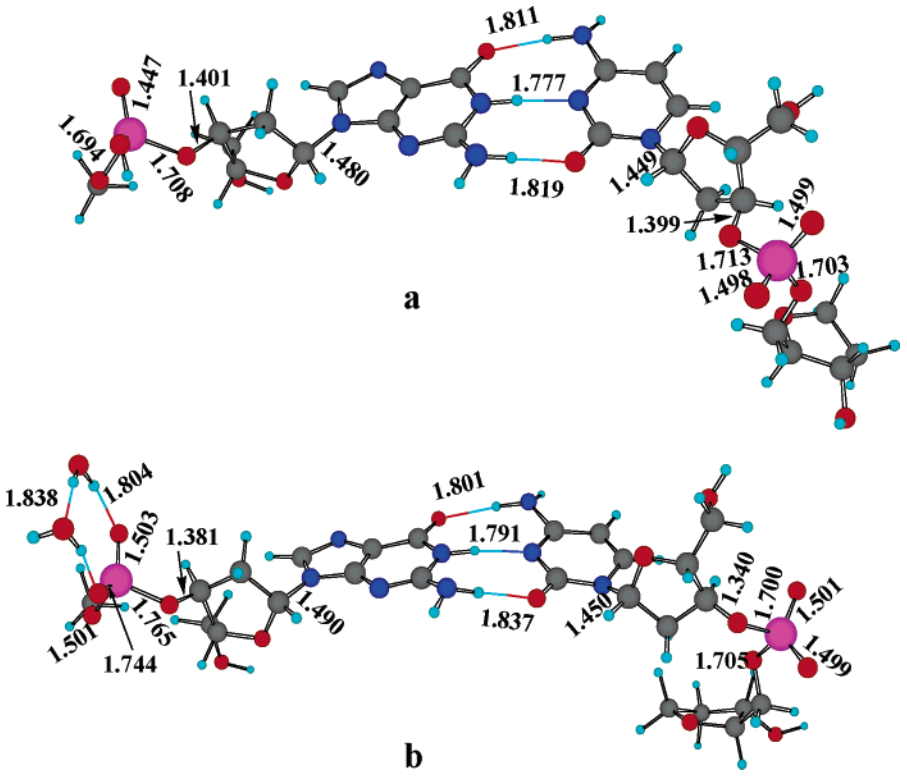

Figure 4. Optimized structures of bare (a) anion (**HPSG••CSP**$^{-}$) and (b) dianion [**$(H_2O)_2$-PSG••CSP**$^{-}$] model systems. All bond lengths are in angstroms.

In the case of the outer-sphere structure of Na^+, the Na−O bonds around the metal ion show a substantial distortion from the tetrahedral arrangement. For instance, in this geometry, the O7−Na−O8 angle is found to be 134.6°, which is quite large compared to a tetrahedral angle. In fact, Na, O6, O7, and O8 atoms are nearly in the same plane as the sum of the angles ∠O6NaO7, ∠O6NaO8, ∠O7NaO8, which is found to be 359.1°. Compared to the Li^+-induced outer-sphere structure, the distortion from tetrahedral arrangement is quite large in the Na^+-induced structure because, in the latter system, the Na−O bond is expected to be weaker than the Li−O bond in the former system. Further, the O5••H−O8 hydrogen-bond interaction between the two metal-bound water molecules (Figure 6a) would also facilitate the tetrahedral distortion in the Na^+-induced structure. Compared to the outer-sphere structure, Na−O bond connections found in the inner-sphere mono- and bidentate structures are largely in a tetrahedral arrangement around the metal (Figure 6b and c), and this feature is also very similar to the corresponding Li^+ geometries.

In the case of K^+, the outer-sphere structure was not found. All attempts to find the outer-sphere coordination always led to the inner-sphere monodentate structure. In the monodentate system, the ∠O7KO5 angle is found to be 164.7° and the sum of the angles ∠O5KO6, ∠O5KO7, and ∠O6KO7 is 359.9°. It means that the arrangement of the K−O bonds in the system is very similar to the arrangement of the Na−O bond in the outer-sphere structure of Na^+. On the other hand, the bidentate structure retained the tetrahedral arrangement of the K−O bonds (Figure 6 e).

The average values of the metal−oxygen distances are 1.971 and 2.288 Å for outer-sphere structures of Li^+ and Na^+, respectively, and those for the inner-sphere monodentate structures are 1.977, 2.302, and 2.694 Å for Li^+, Na^+, and K^+, respectively. Slightly higher values of 2.037, 2.324, 2.691 Å are observed for the average metal−oxygen distances in the bidentate structures of Li^+, Na^+, and K^+, respectively. It can be understood that the average metal−oxygen distances increase with an increase in size of the metal ion. However, it does not change much with respect to the different binding modes preferred by the metal ions. In general, the P−O bond interacting with the hydrated metal (P−O1 and P−O2) showed a small amount of elongation, whereas the other two P−O bonds (P−O3 and P−O4 connected to the sugar unit) showed a small amount of shortening as compared to the corresponding bonds in the free anion (see the SI for detailed bond length information). For instance, the average of P−O1 and P−O2 distances was 1.525 Å, and the average of P−O3 and P−O4 distances was 1.669 Å.

C. Geometries of $(H_2O)_2$ ••$^{-}$PSG••CSP^{-}••$M^+(H_2O)_4$ Dianion Models. The dianion model is selected in order to understand the effect of excess negative charge on the DNA fragment on the metal ion−DNA interaction. The QM regions of the ONIOM-optimized geometries of different binding modes of $Li^+(H_2O)_4$, $Na^+(H_2O)_4$, and $K^+(H_2O)_4$ are presented in Figure 7 (see the SI for the full systems). In the dianion model, the outer-sphere model for Li^+ and the inner-sphere bidentate model for K^+ could not be located. In the case of inner-sphere mono- and bidentate structures of the metals, Li−O bonds are arranged in a tetrahedral fashion around the metal. The outer-sphere Na^+-induced structure is very unique as it shows the arrangement of all four of the oxygen atoms of the water molecules and the

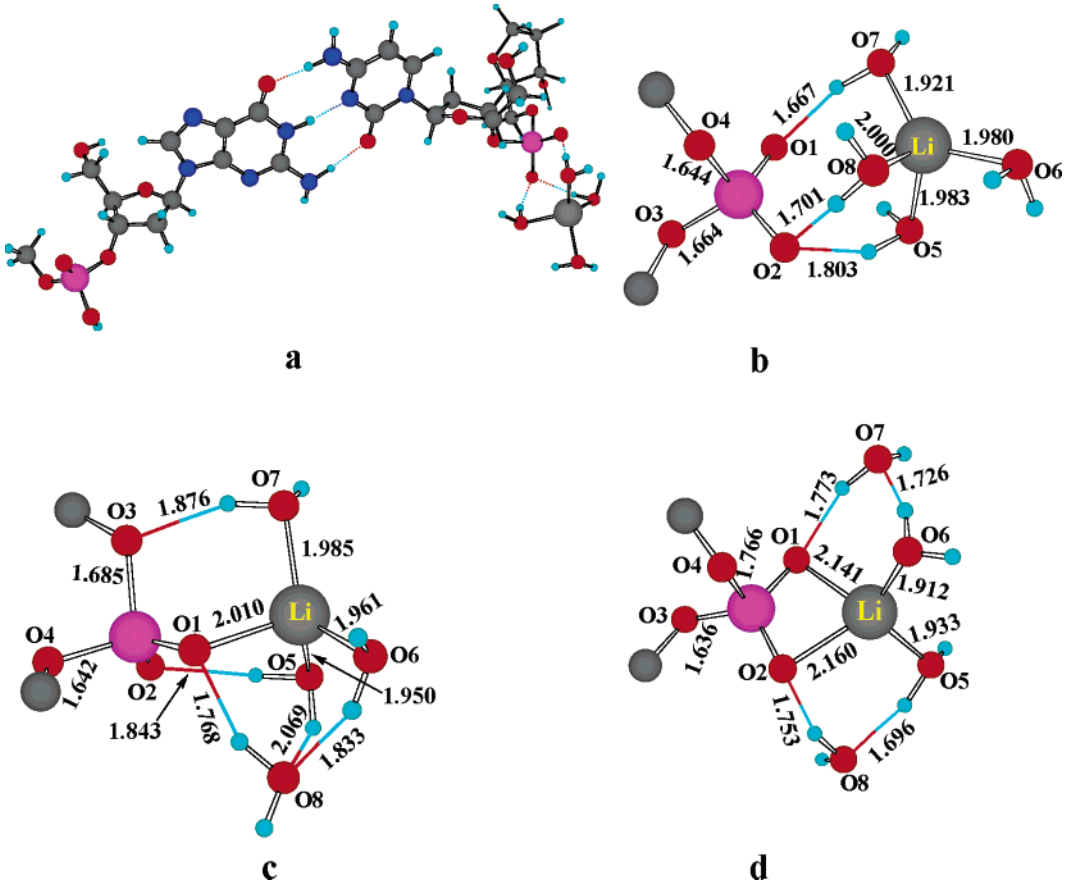

Figure 5. HPS••CSP$^-$••Li$^+$(H$_2$O)$_4$ anion model (a) ONIOM-level optimized full geometry for outer-sphere binding. Parts b, c, and d are the QM region of the ONIOM optimized geometries for outer-sphere binding, inner-sphere monodentate binding, and the inner-sphere bidentate binding, respectively. All bond lengths are in angstroms.

metal in nearly the same plane, meaning that a large distortion from a tetrahedral to a square planar arrangement takes place during the formation of the complex. On the other hand, the tetrahedral arrangement of the Na−O bonds is not much distorted during the formation of the inner-sphere monodentate structure. In both the K$^+$-induced outer-sphere and inner-sphere monodentate structures, the K−O bonds around the metal are largely distorted from the tetrahedral arrangement, and in the former case, the part of the structure defined by four water molecules and the metal can be best described as a square pyramid in which the apical position is occupied by a K atom.

In the dianion structures, the average metal−oxygen distances are 1.964, 2.024, 2.365, 2.291, 2.751, and 2.652 Å for inner-sphere monodentate Li$^+$, inner-sphere bidentate Li$^+$, outer-sphere Na$^+$, inner-sphere monodentate Na$^+$, outer-sphere K$^+$, and inner-sphere monodentate K$^+$, respectively. All of these values are shorter than the corresponding values found in the respective anion models. This means that a tighter metal−phosphate binding is occurring in the dianion model than in the anion models. However, these binding interactions have only a small influence on the exposed P−O bond lengths, as they showed an average distance of 1.515 Å, which is in fact smaller than the corresponding value found in the anion models. On the other hand, compared to anion models, the metal−phosphate binding interaction in the dianion models led to a further shortening of the P−O bonds connected to the sugar units, as they showed an average P−O distance of 1.654 Å.

D. Interaction Energies. The G••C base pair interaction energy data of the three different binding modes (outer-sphere and inner-sphere monodentate and bidentate) of the hydrated alkali metal ions in the dianion model are given in Table 1. For anion and dianion models, eqs 3 and 4 are used to calculate these energies (E3 for anion and E4 for dianion models). It may be seen that, irrespective of the metal ions and their different binding modes, base pair interaction energy in the anion model is nearly close to 25.0 kcal/mol, which is 4.6 kcal/mol smaller than the E1 value of the G••C pair in the free anion model. In the anion models, the average value of the three hydrogen-bond lengths for the G••C base pair is in the range of 1.802−1.805 Å (see the Supporting Information for a distance table), meaning that the hydrogen-bond interactions in all the hydrated metal−anion model systems are nearly unchanged, which is in agreement with the nearly identical interaction energy values. Similarly, in all of the dianion cases, the base pair interaction energy (E4) is nearly identical to 21.0 kcal/mol. However, this E4 value is 4.0 kcal/mol smaller than the E3 value obtained for the anion models, indicating that the excess negative charge on the DNA fragment is weakening the G••C hydrogen-bond strength. On the other hand, compared to the G••C base pair interaction in the free dianion model (E2), the E4 value is 13.7 kcal/mol higher in magnitude. This can be attributed

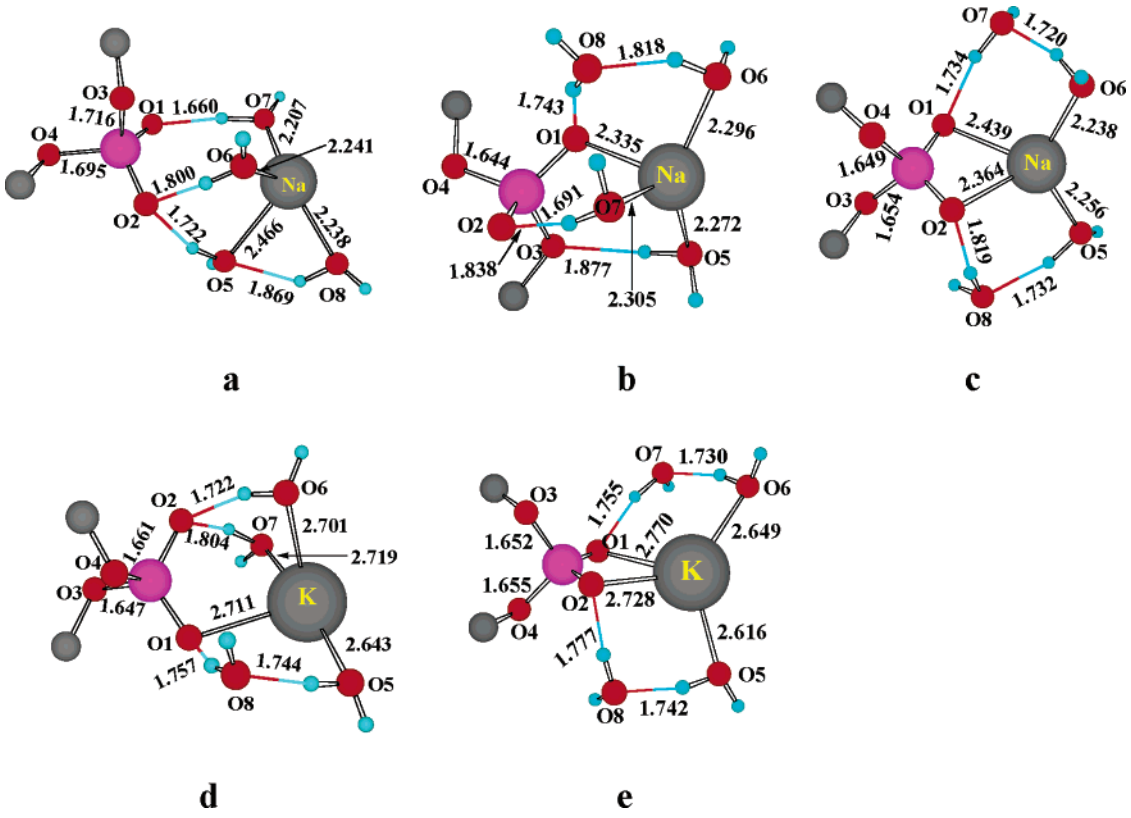

Figure 6. Anion models for HPS••CSP$^-$••Na$^+$(H$_2$O)$_4$ and HPS••CSP$^-$••K$^+$(H$_2$O)$_4$. The QM layer of the ONIOM optimized geometry for (a) outer-sphere binding of Na$^+$ (b and d) inner sphere monodentate binding, and (c and e) the inner sphere bidentate binding. All bond lengths are in angstroms.

mainly to the decrease in the repulsive electrostatic interaction in the dianion−metal system as a result of the neutralization of the charge on the cytosine end. Compared to the anion−metal systems, the average values of the three hydrogen-bond lengths (1.810−1.813 Å) in the G−C pair of dianion−metal systems are increased as a result of the weakening of the G••C base pair interaction.

Table 2 depicts the metal ion−phosphate interaction energy data for tetrahydrated Li$^+$, Na$^+$, and K$^+$ ions with anion and dianion models in the outer-sphere, inner-sphere monodentate, and inner-sphere bidentate binding modes. For anion and dianion models, eqs 5 and 6 are used to calculate these energies (E5 for anion and E6 for dianion models), respectively. In the case of the anion model of lithium, the E5 values show the following order of stability: outer-sphere > inner-sphere monodentate > inner-sphere bidentate. The outer-sphere coordination with a binding energy (BE) of 103.1 kcal/mol is superior to the values of 88.9 and 76.9 kcal/mol obtained for the inner-sphere mono- and bidentate structures, respectively. On the other hand, in the case of the anion model of Na$^+$, all three of the modes of binding have nearly identical strengths, with the inner-sphere bidentate having the highest value of 87.9 kcal/mol for the BE. The anion model of K$^+$ showed the highest stability for the inner-sphere monodentate structure (E5 = 98.2 kcal/mol). As a whole, the E5 values suggest that, in the anion models, the binding strength is in the order Li$^+$ > K$^+$ > Na$^+$.

The energy data of tetrahydrated alkali metal−phosphate anion interactions of the dianion models in Table 2 suggest a substantial increase in the metal phosphate BE in all types of binding modes when compared with the corresponding values obtained in the case of the anion models. For instance, compared to the inner-sphere monodentate anion model, the inner-sphere monodentate dianion model of Li$^+$ showed an increase in the BE by 41%.

In the case of Li$^+$ binding to the dianion model, the E6 values obtained for inner-sphere monodentate and inner-sphere bidentate are 125.7 and 118.9 kcal/mol, respectively, which suggests that Li$^+$ prefers the inner-sphere monodentate binding mode. In contrast, in the anion model, the stable binding mode observed with the Li$^+$ ion was the outer-sphere one, which implies that the charge of the model system is crucial in deciding the type of binding.

The difference in the binding mechanism could be due to the fact that, as the dianion model has higher negative potential, it holds the lithium ion closer to the DNA fragment than the anion fragment accompanied by the removal of water from the hydrated Li$^+$ (dehydration), resulting in an inner-sphere monodentate binding mode. Moreover, in the case of inner-sphere binding, the metal−oxygen distances are shorter than that in the anion model. Unlike lithium, in the case of Na$^+$ and K$^+$, it can be understood from the E6 values that they prefer the outer-sphere binding mode in the dianion model. Whereas in the anion model, the most stable binding mechanisms observed with Na$^+$ and K$^+$ were inner-sphere bidentate and monodentate, respectively. However, it should be noted that the inner-sphere bidentate structure could not be located for Na$^+$ in the dianion model. It can therefore be concluded that the binding modes of alkali metal ions largely depend on the charge of the DNA fragment.

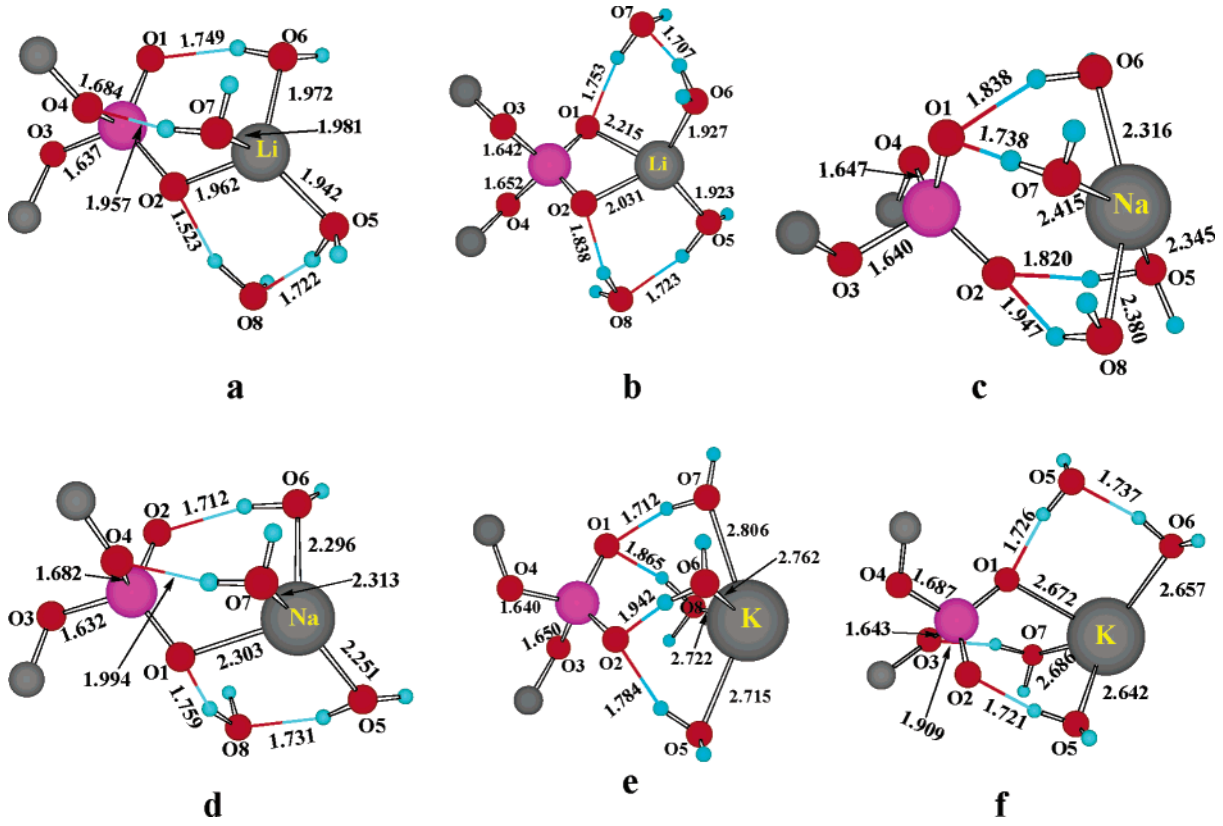

Figure 7. The $[(H_2O)_2\bullet\bullet^{-}PSG\bullet\bullet CSP^{-}\bullet\bullet M^{+}(H_2O)_4]$ dianion models for alkali metal ions. Parts a and b are the inner-sphere mono- and bidentate structures for the Li^+ ion, respectively. Parts c and d are the outer-sphere and inner-sphere monodentate structures of the Na^+ ion, respectively; parts e and f are outer- and inner-sphere monodentate structures for the K^+ ion, respectively. All bond lengths are in angstroms.

Table 1. BSSE-Corrected G••C Base Pair Interaction Energy in Anion (E3) and Dianion (E4) Models[a]

	outer-sphere		inner-sphere monodentate		inner-sphere bidentate	
model systems	E3 (anion)	E4 (dianion)	E3 (anion)	E4 (dianion)	E3 (anion)	E4 (dianion)
Li^+	25.2 (4.7)	not found	25.4 (4.6)	21.0 (4.7)	25.9 (4.7)	20.8 (4.8)
Na^+	24.7 (4.7)	20.5 (4.8)	25.3 (4.6)	20.6 (4.8)	25.1 (4.7)	not found
K^+	not found	20.6 (4.9)	24.9 (4.6)	20.7 (4.9)	25.2 (4.7)	not found

[a] Values in parentheses are the BSSE corrections. All values are in kilocalories per mole.

Table 2. Phosphate−Hydrated Metal Ion Interaction Energy in Anion (E5) and Dianion (E6) Models[a]

	outer-sphere		inner-sphere monodentate		inner-sphere bidentate	
model systems	E5 (anion)	E6 (dianion)	E5 (anion)	E6 (dianion)	E5 (anion)	E6 (dianion)
Li^+	103.1 (9.4)	not found	88.9 (9.9)	125.7 (9.2)	76.9 (11.4)	118.9 (12.8)
Na^+	86.1 (9.1)	118.5 (11.0)	86.4 (9.9)	116.0 (10.5)	87.9 (11.5)	not found
K^+	not found	114.2 (12.6)	98.2 (10.5)	114.6 (9.9)	86.4 (10.5)	not found

[a] Values in parentheses are the BSSE corrections. All values are in kilocalories per mole.

E. Possibilities of Higher Coordination Geometries. In the previous sections, all of the models were made with four water molecules in the first solvation shell of the metal ion. Although this may be a valid assumption, the higher coordination possibilities exist particularly in the case of Na^+ and K^+ ions because of the larger size of their coordination sphere.[54−57] In the case of Li^+, the commonly observed coordination number is four.[58−61] However, there are examples where this cation shows a penta coordination, which mainly arises when it interacts with a multidentate ligand such as a crown ether. In the case of Na^+, octahedral coordination with six nearest-neighbor oxygen interactions is reported in protein structures.[62] In such structures, many of the Na−O interactions are furnished by carboxylate groups of an amino acid residue as well as the carbonyl group of the peptide bond. From a combined quantum chemical statistical simulation study on the hydration of Na^+, Öhrn and Karlström[58] have recently proposed a value close to five

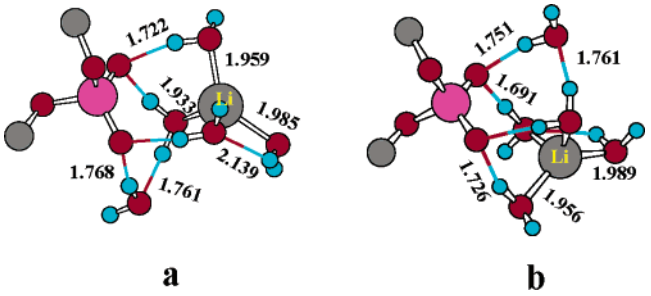

Figure 8. Optimized structures taken from the full model of (a) HPS••CSP$^-$••Li$^+$(H$_2$O)$_5$ and (b) (H$_2$O)$_2$••$^-$PSG••CSP$^-$•• Li$^+$(H$_2$O)$_5$. All bond lengths are in angstroms.

for the average coordination number for Na$^+$, while other workers have reported this value to be around six.[63,64] In the case of K$^+$, coordination numbers even higher than six are located. For instance, in a recent study, Di Cera and co-workers[65] have reported the high-resolution structure of thrombin containing seven K$^+$−O bonding interactions. In the present work, the reported structures in Figures 6a,d and 7c,e,f show a large bare region around the metal center, suggesting further coordination possibilities with water molecules. This aspect is explored to a limited extent by further ONIOM-level calculations on model structures containing five and six water molecules around the metal center.

The initial geometry of the HPS••CSP$^-$••Li$^+$(H$_2$O)$_5$ anion model is made by adding one water molecule to the most stable outer-sphere HPS••CSP$^-$••Li$^+$(H$_2$O)$_4$ complex so that the newly added water is within the Li−O bonding region (∼2.0 Å). Similarly, to the most stable inner-sphere dianion model (H$_2$O)$_2$••$^-$PSG••CSP$^-$ ••Li$^+$(H$_2$O)$_4$, one more water molecule is added in the Li−O bonding region to obtain the (H$_2$O)$_2$••$^-$PSG••CSP$^-$••Li$^+$(H$_2$O)$_5$ dianion system. In both of the cases, the final optimized geometry (Figure 8) showed a tetrahedral coordination of four water molecules around the Li$^+$ and the fifth water molecule was moved out to the second solvation shell. Further addition of water molecules is expected to keep the tetra coordination around the Li$^+$, and therefore their geometries are not optimized.

The initial geometries of HPS••CSP$^-$••Na$^+$(H$_2$O)$_5$ and HPS••CSP$^-$••Na$^+$(H$_2$O)$_6$ models for ONIOM optimization are made by adding the appropriate number of water molecules at the Na−O bonding distances (2.3 Å). The same strategy is used in the case of dianion models as well (cf. Figure 9 for optimized structures). The anion model HPS••CSP$^-$••Na$^+$(H$_2$O)$_5$ turns out to be an inner-sphere monodentate structure wherein only three of the water molecules showed strong coordination to the metal ion. On the other hand, the dianion model showed the outer-sphere coordination with four strong Na−O bonding interactions. In this case, the fifth water molecule is moved out from the coordination sphere to keep hydrogen-bonding interactions with one of the phosphate oxygen atoms and another water in the first solvation shell. Although HPS••CSP$^-$••Na$^+$(H$_2$O)$_5$ is described as an outer-sphere structure, the Na−O$_{(phosphate)}$ distance of 2.579 Å suggests significant interaction between the corresponding atoms. The anion and the dianion models with six water molecules possess outer-sphere coordination,

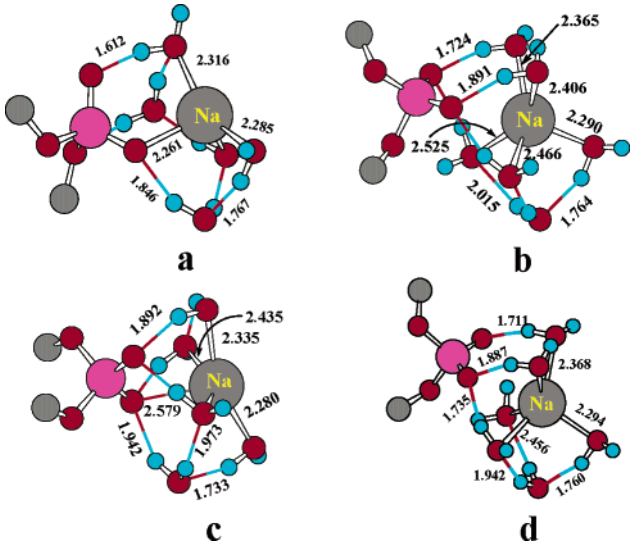

Figure 9. Optimized structures taken from the full model of (a) HPS••CSP$^-$••Na$^+$(H$_2$O)$_5$, (b) HPS••CSP$^-$••Na$^+$(H$_2$O)$_6$, (c) (H$_2$O)$_2$••$^-$PSG••CSP$^-$••Na$^+$(H$_2$O)$_5$, and (d) (H$_2$O)$_2$••$^-$PSG•• CSP$^-$••Na$^+$(H$_2$O)$_6$. All bond lengths are in angstroms.

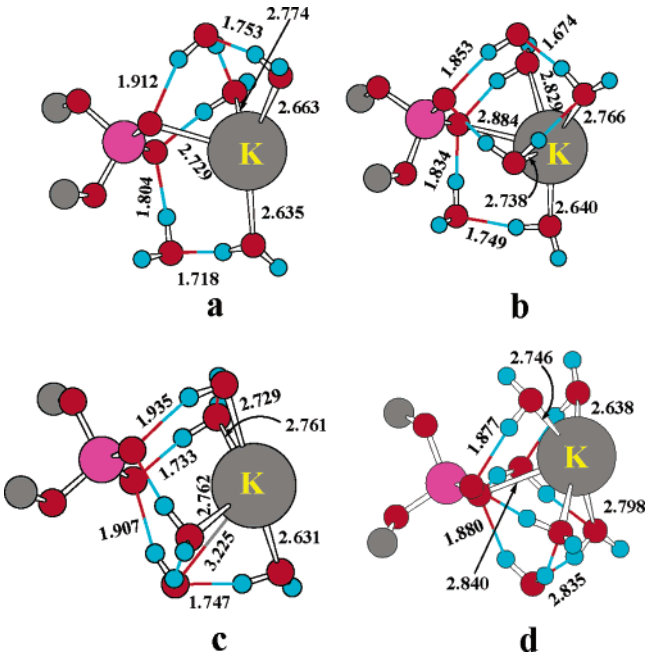

Figure 10. Optimized structures taken from the full model of (a) HPS••CSP$^-$••K$^+$(H$_2$O)$_5$, (b) HPS••CSP$^-$••K$^+$(H$_2$O)$_6$, (c) (H$_2$O)$_2$••$^-$PSG••CSP$^-$••K$^+$(H$_2$O)$_5$, and (d) (H$_2$O)$_2$••$^-$PSG•• CSP$^-$••K$^+$(H$_2$O)$_6$. All bond lengths are in angstroms.

and both of the structures are nearly identical, showing direct coordination of five water molecules to the metal center. In this case, the nearest Na−O$_{(phosphate)}$ distance is found to be 2.840 Å.

For the systems containing K$^+$, further additions of water molecules are carried out with the inner-sphere HPS••CSP$^-$••K$^+$(H$_2$O)$_4$ (cf. Figure 6d) and the outer-sphere (H$_2$O)$_2$••$^-$PSG••CSP$^-$••K$^+$(H$_2$O)$_4$ models (cf. Figure 7e). The ONIOM-level optimized geometries are presented in Figure 10. Both of the anion models (with five and six water molecules) show inner-sphere monodentate coordination of the metal ion to the phosphate. In HPS••CSP$^-$••K$^+$(H$_2$O)$_5$,

Table 3. Phosphate−Hydrated Metal Ion Interaction Energy in Anion and Dianion Models[a]

	anion		dianion	
model systems	E7 for $M^+(H_2O)_5$	E8 for $M^+(H_2O)_6$	E9 for $M^+(H_2O)_5$	E10 for $M^+(H_2O)_6$
Li^+	98.1 (10.5)		121.1 (10.4)	
Na^+	87.9 (11.1)	85.5 (12.0)	117.3 (11.8)	117.0 (12.1)
K^+	96.2 (11.7)	97.6 (12.2)	115.6 (12.5)	114.1 (14.1)

[a] Values in parentheses are the BSSE corrections. All values are in kilocalories per mole.

three water molecules are directly bonded to the K^+, while in HPS••CSP$^-$••$K^+(H_2O)_6$, four water molecules show strong interaction with the K^+. Interestingly, the $(H_2O)_2$••$^-$PSG••CSP$^-$••$K^+(H_2O)_5$ dianion model possesses outer-sphere coordination while the $(H_2O)_2$••$^-$PSG••CSP$^-$••$K^+(H_2O)_6$ is inner-sphere monodentate. In both of the dianion systems, four water molecules are directly bonded to the metal center. It may be noted that, even with five or six water molecules, full coverage of the coordination sphere of both Na^+ and K^+ is not achieved. Interestingly, these metal centers are unable to keep six M^+−O-type bonding interactions, and it is felt that through the mediation of water molecules in the secondary solvation shell such coordination may arise. For instance, in HPS••CSP$^-$••$Na^+(H_2O)_6$, the water molecule in the secondary solvation shell (cf. Figure 9b) is helpful to maintain the rigidity of the penta-coordinated metal ion in it.

The BSSE-corrected BE values E7, E8, E9, and E10 are calculated to quantify the interaction of the hydrated metal ion to the phosphate moiety (Table 3). E7 and E8 represent the interaction of $M^+(H_2O)_5$ and $M^+(H_2O)_6$ with the anion, while E9 and E10 represent the interaction of $M^+(H_2O)_5$ and $M^+(H_2O)_6$ with the dianion, respectively. A comparison of the energy values in Tables 2 and 3 suggests that, in the case of Li^+, the maximum BE to both the anion and the dianion is obtained when it is hydrated with four water molecules. Similarly, dianion models containing $Na^+(H_2O)_4$ and the anion model containing $K^+(H_2O)_4$ show more BE than their corresponding penta- and hexa-hydrated metal centers. In contrast to this, in the anion models, the penta-hydrated Na^+ system shows binding strength equal to that of the tetra-hydrated inner-sphere bidentate structure (BE = 87.9 kcal/mol). Among all the dianion models of K^+, the $(H_2O)_2$••$^-$PSG••CSP$^-$••$K^+(H_2O)_5$ system has the highest BE (115.6 kcal/mol).

IV. Conclusions

The interactions of hydrated Li^+, Na^+, and K^+ ions to the phosphate group of DNA are studied by modeling a DNA fragment both in an anion (one negative charge) and a dianion (two negative charges) state with the phosphate geometry maintained as in native DNA (projected toward the exterior) using a three-layer ONIOM-based QM−MM method. Three combinations of metal ion−DNA binding were studied, which included the outer-sphere, inner-sphere monodentate, and inner-sphere bidentate patterns. Among the alkali metal ions, Li^+ is known to have the highest affinity for DNA in aqueous solutions in terms of counterion interactions.[66] The present results are in good agreement with this as, among all the structures, Li^+ showed the highest BE in both anion and dianion models, where the former is of 103.1 kcal/mol [outer-sphere HPS••CSP$^-$••$Li^+(H_2O)_4$] and the latter is 125.7 kcal/mol [inner-sphere monodentate $(H_2O)_2$••$^-$PSG••CSP$^-$ ••$Li^+(H_2O)_4$]. Comparison of all the structures with the highest BE shows that the binding strength of the metal ions follows the order $Li^+ > K^+ > Na^+$ in the anion models, while it is $Li^+ > Na^+ > K^+$ in the dianion models. Experimental reports have shown that Li^+ ions prefer outer-sphere binding to DNA[16] and stabilizes the water structure around DNA,[50] and Na^+ and K^+ ions bind to DNA in an inner-sphere manner,[14,15] which is in good agreement with the binding behavior of these ions with the anion model, as the structures with the highest binding energies are outer-sphere HPS••CSP$^-$••$Li^+(H_2O)_4$, inner-sphere monodentate HPS••CSP$^-$••$Na^+(H_2O)_5$, and inner-sphere monodentate HPS••CSP$^-$••$K^+(H_2O)_4$. This suggests that the neutral anion model is quite suitable for studying the interactive behavior of alkali metal ions compared to the dianion model where the net charge on the system is not neutral. In the dianion models, the Coulombic electrostatic interaction between the dianion system and the positively charged hydrated metal ion is higher than that of the anion system and the hydrated metal ions. Therefore, all dianion models showed a higher binding energy than the anion models. It appears that, when the net charge on the DNA−metal system is not zero, the results are not in agreement with the experiment. Our previous work[53] on the binding behavior of alkaline earth metals (dipositively charged) on a DNA fragment revealed similar results where only the dianion model having net zero charge showed the right binding behavior, as found in the experiments.

Acknowledgment. We thank the Council of Scientific and Industrial Research, Government of India, for the support of this work. We also thank Dr. C. K. S. Pillai for fruitful discussions.

Supporting Information Available: Optimized geometries of all the structures and a discussion on the hydrated metal ions. This material is available free of charge via the Internet at http://pubs.acs.org.

References

(1) Eichhorn, G. L. *Adv. Inorg. Biochem.* **1981**, *3*, 1.

(2) Martin, R. B. *Acc. Chem. Res.* **1985**, *18*, 32.

(3) Saenger, W. *Principles of Nucleic Acid Structure*; Springer-Verlag: New York, 1994.

(4) Sigel, H. *Chem. Soc. Rev.* **1993**, *22*, 255.

(5) Glusker, J. P. *Adv. Protein Chem.* **1991**, *42*, 1.

(6) Misra, V. K.; Draper, D. E. *Biopolymers* **1998**, *48*, 113.

(7) Alexander, R. S.; Kanyo, Z. F.; Chirlian, L. E.; Christianson, D. W. *J. Am. Chem. Soc.* **1990**, *112*, 933.

(8) Laughton, C. A.; Luque, F. J.; Orozco, M. *J. Phys. Chem.* **1995**, *99*, 11591.

(9) Schneider, B. K.; Kabelac, M.; Hobza, P. *J. Am. Chem. Soc.* **1996**, *118*, 12207.

(10) Bamann, E.; Trapmann, H.; Fischler, F. *Biochem. Z.* **1954**, *328*, 89.

(11) Marzilli, L. G.; Kistenmacher, T. J.; Eichhorn, G. L. *Nucleic Acid-Metal Ion Interactions*; John Wiley and Sons: New York, 1980; Vol. 1.

(12) Missailides, S.; Anastassopoulou, J.; Fotopoulos, N.; Theophanides, T. *Asian J. Phys.* **1997**, *6*, 481.

(13) Chiu, T. K.; Dickerson, R. E. *J. Mol. Biol.* **2000**, *301*, 915.

(14) Tereshko, V.; Wilds, C. J.; Minasov, G.; Prakash, T. P.; Maier, M. A.; Howard, A.; Wawrzak, Z.; Manoharan, M.; Egli, M. *Nucleic Acids Res.* **2001**, *29*, 1208.

(15) Stelwagen, N. C.; Magnusdottir, S.; Gelfi, C.; Righeti, P. G. *J. Mol. Biol.* **2001**, *305*, 1025.

(16) Zheng, J.; Li, Z.; Wu, A.; Zhou, H. *Biophys. Chem.* **2003**, *104*, 37.

(17) Hamelberg, D.; McFail-Isom, L.; Williams, L. D.; Wilson, W. D. *J. Am. Chem. Soc.* **2000**, *122*, 10513.

(18) Feig, M.; Pettitt, B. M. *Biophys. J* **1999**, *77*, 1769.

(19) Sigel, H. *Metal-DNA Chemistry*; American Chemical Society: Washington, D. C., 1989; Vol. 159.

(20) Sponer, J.; Burda, J. V.; Leszczynski, J.; Hobza, P. *J. Biomol. Struct. Dyn.* **1999**, *17*, 61.

(21) Sponer, J.; Hobza, P. *Collect. Czech. Chem. Commun.* **2003**, *68*, 2231.

(22) Sponer, J.; Leszczynski, J.; Hobza, P. *THEOCHEM* **2001**, *573*, 43.

(23) Sponer, J.; Sabat, M.; Burda, J. V.; Leszczynski, J.; Hobza, P.; Lippert, B. *J. Biol. Inorg. Chem.* **1999**, *4*, 537.

(24) Sponer, J. E.; Sychrovsky, V.; Hobza, P.; Sponer, J. *Phys. Chem. Chem. Phys.* **2004**, *6*, 2772.

(25) Munoz, J.; Sponer, J.; Hobza, P.; Orozco, M.; Luque, F. J. *J. Phys. Chem. B* **2001**, *105*, 6051.

(26) Petrov, A. S.; Funseth-Smotzer, J.; Pack, G. R. *Int. J. Quantum Chem.* **2005**, *102*, 645.

(27) Petrov, A. S.; Lamm, G.; Pack, G. R. *J. Phys. Chem. B* **2002**, *106*, 3294.

(28) Petrov, A. S.; Lamm, G.; Pack, G. R. *J. Phys. Chem. B* **2004**, *108*, 6072.

(29) Bandyopadhyay, D.; Bhattacharya, D. *J. Biomol. Struct. Dyn.* **2003**, *21*, 447.

(30) Bertran, J.; Rodriguez-Santiago, L.; Sodupe, M. *J. Phys. Chem. B* **1999**, *103*, 2310.

(31) Zeizinger, N.; Burda, J. V.; Sponer, J.; Kapsa, V.; Leszczynski, J. *J. Phys. Chem. A* **2001**, *105*, 8086.

(32) Murashov, V. V.; Leszczynski, J. *J. Phys. Chem. B* **1999**, *103*, 8391.

(33) Rodger, A.; Sanders, K. J.; Hannon, M. J.; Meistermann, I.; Parkinson, A.; Vidler, D. S.; Haworth, I. S. *Chirality* **2000**, *12*, 221.

(34) Marincola, F. C.; Denisov, V. P.; Halle, B. *J. Am. Chem. Soc.* **2004**, *126*, 6739.

(35) Kankia, B. I. *Biopolymers* **2004**, *74*, 232.

(36) Jerkovic, B.; Bolton, P. H. *Biochemistry* **2001**, *40*, 9406.

(37) Svensson, M.; Humbel, S.; Froese, R. D. J.; Matsubara, T.; Sieber, S.; Morokuma, K. *J. Phys. Chem.* **1996**, *100*, 19357.

(38) Humbel, S.; Sieber, S.; Morokuma, K. *J. Chem. Phys.* **1996**, *105*, 1959.

(39) Dapprich, S.; Komaromi, I.; Byun, K. S.; Morokuma, K.; Frisch, M. J. *THEOCHEM* **1999**, *461*−*462*, 1.

(40) Tschumper, G. S.; Morokuma, K. *THEOCHEM* **2002**, *592*, 137.

(41) Re, S.; Morokuma, K. *J. Phys. Chem. A* **2001**, *105*, 7185.

(42) Becke, A. D. *J. Chem. Phys.* **1993**, *98*, 5648.

(43) Becke, A. D. *Phys. Rev. A: At., Mol., Opt. Phys.* **1988**, *38*, 3098.

(44) Hariharan, P. C.; Pople, J. A. *Mol. Phys.* **1974**, *27*, 209.

(45) Stewart, J. J. P. *J. Comput. Chem.* **1989**, *10*, 209.

(46) Rappé, A. K.; Casewit, C. J.; Colwell, K. S.; Goddard, W. A., III; Skiff, W. M. *J. Am. Chem. Soc.* **1992**, *114*, 10024.

(47) Glendening, E. D.; Feller, D. *J. Phys. Chem.* **1995**, *99*, 3060.

(48) Egli, M. *Chem. Biol.* **2002**, *9*, 277.

(49) Boys, S. F.; Bernardi, F. *Mol. Phys.* **1970**, *19*, 553.

(50) Campbell, N. H.; Evans, D. A.; Lee, M. P.; Parkinson, G. N.; Neidle, S. *Bioorg. Med. Chem. Lett.* **2006**, *16*, 15.

(51) Hays, F. A.; Teegarden, A. T.; Jones, Z. J. R.; Harms, M.; Raup, D.; Watson, J.; Cavaliere, E.; Ho, P. S. *Proc. Natl. Acad. Sci. U.S.A.* **2005**, *102*, 7157.

(52) Sponer, J.; Jurecka, P.; Hobza, P. *J. Am. Chem. Soc.* **2004**, *126*, 10142.

(53) Sundaresan, N.; Pillai, C. K. S.; Suresh, C. H. *J. Phys. Chem. A* **2006**, *110*, 8826.

(54) Jungwirth, P.; Tobias, D. J. *J. Phys. Chem. B* **2002**, *106*, 6361.

(55) Várnai, P.; Zakrzewska, K. *Nucleic Acids Res.* **2004**, *32*, 4269.

(56) Draper, D. E.; Grilley, D.; Soto, A. M. *Annu. Rev. Biophys. Biomol. Struct.* **2005**, *34*, 221.

(57) Hud, N. V.; Smith, F. W.; Anet, F. A. L.; Feigon, J. *Biochemistry* **1996**, *35*, 15383.

(58) Öhrn, A.; Karlström, G. *J. Phys. Chem. B* **2004**, *108*, 8452.

(59) Obst, S.; Bradaczek, H. *J. Phys. Chem.* **1996**, *100*, 15677.

(60) Loeffler, H. H. R. B. M. *J. Chem. Phys.* **2002**, *117*, 110.

(61) Duan, Z. H.; Zhang, Z. G. *Mol. Phys.* **2003**, *101*, 1501.

(62) Nayal, M.; Di Cera, E. *J. Mol. Biol.* **1996**, *256*, 228.

(63) Tòth, G. *J. Chem. Phys.* **1996**, *105*, 5518.

(64) Degrève, L.; de Pauli, V. M.; Duarte, M. A. *J. Chem. Phys.* **1997**, *106*, 655.

(65) Carrell, C. J.; Bush, L. A.; Mathews, F. S.; Di Cera, E. *Biophys. Chem. 121*, 177.

(66) Lyubartsev, A. P.; Laaksonen, A. J. *Biomol. Struct. Dyn.* **1998**, *16*, 579.

CT600245W